Available online at www.sciencedirect.com

ScienceDirect

IFAC Papers Online CONFERENCE PAPER ARCHIVE

IFAC PapersOnLine 56-2 (2023) 7276–7281

Modeling and Control of a Magnetic Levitation Platform

Hans Alvar Engmark * **Kiet Tuan Hoang** *

* *Department of Engineering Cybernetics, The Norwegian University of Science and Technology (NTNU). E-mail: hans.a.engmark@ntnu.no, kiet.t.hoang@ntnu.no*

Abstract: We present two models for a specific class of magnetic levitation system, a type of planar magnetic motor, designed for magnetic levitation of a single permanent magnet using a combination of permanent magnets and electromagnets. The first model is based on established semi-analytical solutions for magnetic fields generated by ideal solenoids, while the second model employs a novel discretization that is well suited for real-time control. Simulations show that the models have comparable accuracy to a standard filament model, but with a reduction in computational time of up to 98 %, for the discretized model. A simulation study demonstrates the models' applicability for advanced control, using a linear-quadratic regulator (LQR) for stable levitation, and a nonlinear model predictive controller (NMPC) to showcase novel control behavior.

Keywords: Mathematical Modeling, Planar Magnetic Actuators, Model Predictive Control

1. INTRODUCTION

The concept of magnetic levitation has intrigued industries for decades. High-speed trains, such as the Chuo Shinkansen, serve as a prime example of its application (Uno, 2016), with other fields as diverse as protein analysis and disease diagnosis (Rahmani Dabbagh et al., 2021), to mechanical energy harvesters (Carneiro et al., 2020), also benefiting from the technology. Despite the variety of systems utilizing magnetic levitation, all such systems are inherently unstable and need some form of stabilizing control. This, in turn, implies the need for dynamical models. Advanced control for magnetic levitation has primarily been limited to a simple class of systems where a magnetic object is hovering *beneath* actively controlled electromagnets, as demonstrated in Trumper et al. (1997); Cho et al. (1993); Bächle et al. (2013) using feedback linearizing-, sliding mode-, and nonlinear model predictive control.

In this paper, we consider the complementary system, illustrated in Fig. 1, where a permanent magnet is hovering *above* a base of solenoids and permanent magnets. This configuration is popular as a display for small items, and to the best of our knowledge it has garnered limited academic attention. However, the many challenges following with its functionality suggest it has untapped potential as a valuable teaching tool for aspiring control engineers. Consequently, this paper aims to develop models suitable for controlling such systems. We here thus consider a maglev system that resembles a *planar magnetic motor*, often employed as a versatile translation device in high-precision manufacturing (Jansen et al., 2014). The main challenge in modeling planar magnetic motors lies in modeling the magnetic fields and forces acting on the levitating magnet. Numerical software is typically required to solve a set of partial differential equations used to describe the system

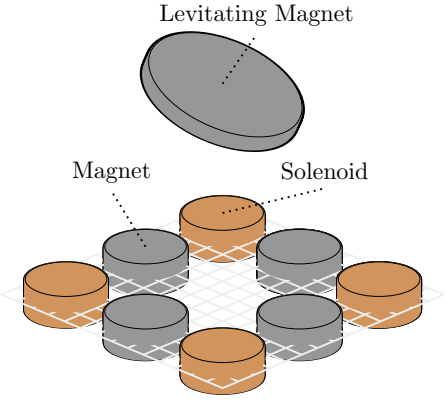

Fig. 1. Illustration of the magnetic levitation system.

(using, e.g., Finite Element Analysis (FEA)) (Berkelman and Dzadovsky, 2013; Jansen et al., 2014). However, here we develop a new mathematical model of the system illustrated in Fig. 1 using efficient semi-analytic solutions of the magnetic fields generated by ideal solenoids and thin wire loops. Additionally, we propose a simple yet effective discretization to develop another model with comparable accuracy but lower computational cost (Wang and Ren, 2014). The novelty of this study lies in the adaptation of literature for the two models and the derivation of a new model for real-time simulations and advanced control. Two control examples are thus presented; 1) a linear-quadratic regulator (LQR) for stabilization, and 2) a nonlinear model predictive controller (NMPC) to showcase novel control behavior.

The manuscript is structured as follows: Section 2 provides the mathematical background and the two proposed models. Section 3 demonstrates the models in open- and closed-loop control using LQR and NMPC controllers. Section 4 discusses some concluding remarks and further works.

10.1016/j.ifacol.2023.10.338

2. MODEL DESCRIPTION

This section presents two *semi-analytic* models for the magnetic levitation system shown in Fig. 1; *Model 1*, prioritizing accuracy, and *Model 2*, prioritizing speed.

The modeling process is divided into three parts: 1) magnetic field (Subsection 2.2), 2) magnetic force and torque (Subsection 2.3), and 3) translation and rotation (Subsection 2.4). This section addresses the modeling of these three components in order, outlining key assumptions and considerations. We follow a bottom-up approach, where later expressions rely on previous ones, and a complete model comprises a collection of the terms presented throughout the paper.

For improved readability, equations that are part of the models are highlighted depending on whether they are used only in ***Model 1***, only in ***Model 2***, or if they are used in ***both models***.

2.1 Modeling Assumptions and Simplifications

The most important modeling assumptions applied are:

(1) Solenoid electrodynamics can be neglected.
This assumption is valid as long as the electrodynamics of the solenoids are significantly faster than the dynamics of the levitating magnet.
(2) Relative permeability of every components is $\mu \approx 1$.
This assumption is valid since solenoids and permanent magnets are typically made of copper ($\mu = 0.995$) and neodymium-iron-boron ($\mu = 1.05$), as opposed to iron ($\mu = 2 \times 10^5$).

Besides these assumptions the models take advantage of the fact that cylindrical uniformly magnetized permanent magnets can be equivalently modeled by ideal thin-walled solenoids of the same radius. This is known as the "equivalent magnetization current" model (Lemarquand et al., 2009; Zhang et al., 2019).

2.2 Magnetic Field

A crucial aspect of modeling magnets is describing the magnetic field $\boldsymbol{H}$ and the magnetic flux density $\boldsymbol{B}$ of the magnet. When the relative permeability of the environment $\mu = 1$, as in Assumption (2), these two quantities are related as $\boldsymbol{B} = \mu_0 \boldsymbol{H}$ (Sadiku and Nelatury, 2001), where μ_0 is the permeability of vacuum. Therefore, only the magnetic flux density $\boldsymbol{B}$ is considered in the following.

Cylindrical Solenoids The magnetic field generated by electrical current running through a wire is described by Biot-Savart's law. In general, there are no analytical solutions to the integrals provided by this law, but, when considering the magnetic field around a thin current-carrying wire loop, there exists semi-analytical solutions of the field, requiring only the numerical solution of a couple of well known integrals. Thus, it is common to model cylindrical solenoids as collections of these loops, one for each turn in the solenoid, which is known as the *filament method* (Ravaud et al., 2010). While this approach yields fairly accurate and efficient computations, it still necessitates solving a large number of semi-analytical integrals.

An alternative approach is to assume that the solenoid is ideal, which means that the coils are tightly wound and located at the same radial position. This assumption is reasonable when the solenoid is thin, or when the magnetic field is measured far from the solenoid (Husa et al., 2020). In this case, the solenoid can be represented as a thin sheet of current that wraps around the outside of the cylinder, for which there also exist semi-analytical solutions.

The field produced by a cylindrical current sheet is given by (Derby and Olbert, 2010)

$$\boldsymbol{B}(\phi,\rho,z) = \begin{bmatrix} \phi \\ c\frac{2R(k^2-2)}{k}\left[\mathrm{K}\left(k^2\right) - \frac{2}{2-k^2}\mathrm{E}\left(k^2\right)\right] \\ c\zeta k\left[\mathrm{K}\left(k^2\right) - \frac{\rho-R}{\rho+R}\Pi\left(h^2,k^2\right)\right] \end{bmatrix}\Bigg|_{\zeta_-}^{\zeta_+} \tag{1a}$$

where

$$k^2 = \frac{4R\rho}{(R+\rho)^2+\zeta^2}, \quad h^2 = \frac{4R\rho}{(R+\rho)^2}$$
$$c = \frac{\mu_0}{4\pi\sqrt{R\rho}}\frac{NI}{l}, \quad \zeta_\pm = z \pm \frac{l}{2}$$

For $\rho = 0$:

$$\boldsymbol{B}(\phi,\rho,z) = \begin{bmatrix} 0 \\ 0 \\ \frac{\mu_0 \zeta N I}{2l\sqrt{R^2+\zeta^2}} \end{bmatrix}\Bigg|_{\zeta_-}^{\zeta_+} \tag{1b}$$

where R and l are the radius and length of the solenoid, (ϕ,ρ,z) are cylindrical coordinates relative to the center of the solenoid, I is the current in the solenoid, N is the number of windings in the solenoid, and $\mathrm{K},\mathrm{E},\Pi$ are the complete elliptical integrals of the first-, second- and third-kind, respectively. The limit case for the field along the axis of the cylindrical magnet is given in (1b).

The solenoids can be approximated by single thin wire loops instead of current sheets to reduce the computational speed further. The field produced by a thin wire loop is (González and Cárdenas, 2020)

$$\boldsymbol{B}(\phi,\rho,z) = \begin{bmatrix} \phi \\ -\frac{z}{\rho}ck\left[\mathrm{K}(k^2) - \frac{\rho^2+R^2+z^2}{(\rho-R)^2+z^2}\mathrm{E}(k^2)\right] \\ ck\left[\mathrm{K}(k^2) - \frac{\rho^2-R^2+z^2}{(\rho-R)^2+z^2}\mathrm{E}(k^2)\right] \end{bmatrix} \tag{2a}$$

where

$$k^2 = \frac{4R\rho}{(R+\rho)^2+z^2}$$
$$c = \frac{\mu_0}{4\pi\sqrt{R\rho}}NI$$

For $\rho = 0$:

$$\boldsymbol{B}(\phi,\rho,z) = \begin{bmatrix} 0 \\ 0 \\ \frac{\mu_0 R^2 N I}{2(R^2+z^2)^{3/2}} \end{bmatrix} \tag{2b}$$

where R is the radius of the loop. Note that l is no longer present.

The surface and thin wire representations are shown compared to the filament method in Fig. 2.

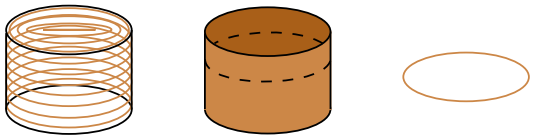

Fig. 2. Different model representations of the solenoids. **From left-to-right:** Filament model, thin current sheet model (Model 1), thin wire loop model (Model 2).

For both the current sheet and thin wire loop representations, accuracy can be improved by adjusting the radius used in the models to make the field in a chosen area more closely resemble the field produced by, e.g., the filament method. For instance, assuming that the true and estimated fields are given by $\boldsymbol{B}, \widehat{\boldsymbol{B}} \quad \forall \rho, z \in \mathcal{D}$, respectively, where $\mathcal{D}$ is some region of interest, a radius $\widehat{R}$ that improves $\widehat{\boldsymbol{B}}$ can be found by

$$\widehat{R} = \text{argmin}_{R \in \mathbb{R}} \left\| \boldsymbol{B} - \widehat{\boldsymbol{B}} \right\|_2^2 \tag{3}$$

Axially Magnetized Cylindrical Permanent Magnets The magnetic fields of the permanent magnets are modeled using the *equivalent magnetization current* approach. The magnetization surface current $\boldsymbol{K}$ $[A/m]$ of a cylindrical magnet is (Ravaud et al., 2010)

$$\boldsymbol{K} = \frac{\boldsymbol{J} \times \boldsymbol{n}}{\mu_0} \tag{4}$$

where $\boldsymbol{J}$ is the magnetic polarization, $\boldsymbol{n}$ is the normal vector to $\boldsymbol{J}$, and μ_0 is the permeability in a vacuum.

The model for the field around an ideal thin wall solenoid, shown in (1), *exactly* represents the field of a cylindrical permanent magnet. Thus, the field produced by a permanent magnet of radius R at a point (ϕ, ρ, z) from its center can be found by using $I = \boldsymbol{K}l$, and $N = 1$ in (1) – or approximated by doing the same with (2).

Total Magnetic Field The expressions in (1) and (2) are given in *cylindrical coordinates*. However, the fields from each component, $\boldsymbol{B}(\phi, \rho, z) = [B_\phi, B_\rho, B_z]^T$, can be equivalently defined in *Cartesian coordinates* as

$$\boldsymbol{B}(x, y, z) = \begin{bmatrix} B_\rho \cos B_\phi \\ B_\rho \sin B_\phi \\ B_z \end{bmatrix} \tag{5}$$

where

$$\rho = \sqrt{x^2 + y^2}, \quad \phi = \arctan \frac{y}{x}$$

Using (5), the total magnetic field produced by the base in *Cartesian coordinates*, (x, y, z), is given by

$$\boldsymbol{B}_{base}(x, y, z) := \sum_{i=1}^{n_s+n_m} \boldsymbol{B}(x - x_i, y - y_i, z - z_i) \tag{6}$$

where (x_i, y_i, z_i) are the Cartesian coordinates of the center of the i'th solenoid/permanent magnet, and n_s and n_m are the total numbers of solenoids and permanent magnets, respectively. Note that $\boldsymbol{B}_{base}$ also depends on the currents in the solenoids ($\boldsymbol{u}$ in the complete model description). However, for ease of notation, it is assumed to be tacit.

2.3 Force & Torque

The force and torque on a permanent magnet of zero size in a uniform magnetic field are (Sadiku and Nelatury, 2001)

$$\begin{aligned} \boldsymbol{F} &= \nabla \left(\frac{\boldsymbol{J}}{\mu_0} \cdot \boldsymbol{B} \right) \\ \boldsymbol{\tau} &= \frac{\boldsymbol{J}}{\mu_0} \times \boldsymbol{B} \end{aligned} \tag{7}$$

where $\boldsymbol{B}$ is the magnetic field strength and $\boldsymbol{J}$ is the magnetic polarization of the magnet. To compute the force and torque on an arbitrary permanent magnet in a heterogeneous magnetic field, one can integrate (7) over the volume of the magnet. Adopting the equivalent magnetization current model mentioned in Section 2.1, this integral can be accurately computed through a surface integral over the equivalent ideal solenoid representation of the permanent magnet, with the equivalent magnetization current $\boldsymbol{I} = \boldsymbol{K}l$ given by (4). The force produced on the levitating magnet by the magnetic field of the base becomes

$$\begin{aligned} \boldsymbol{F} &= \int_{\boldsymbol{S}} \boldsymbol{K}(\alpha, \beta, \gamma) \times \boldsymbol{B}_{base}(x, y, z) \, d\boldsymbol{S} \\ \boldsymbol{\tau} &= \int_{\boldsymbol{S}} \frac{1}{\mu_0} \boldsymbol{J}(\alpha, \beta, \gamma) \times \boldsymbol{B}_{base}(x, y, z) \, d\boldsymbol{S} \end{aligned} \tag{8}$$

where (x, y, z) and (α, β, γ) describe the position and orientation (around itself) of the center of the magnet. The surface S of the levitating magnet depends on the position and orientation.

In practice, (8) has to be solved through numerical integration. Since computing the magnetic field, $\boldsymbol{B}_{base}$, already requires solving elliptical integrals, performing the force and torque integrals will be relatively slow. To alleviate this, the following approximation is proposed

$$\begin{aligned} \boldsymbol{F} &= \frac{2\pi R l}{n} \sum_{i=1}^{n} \boldsymbol{K}(\alpha, \beta, \gamma) \times \boldsymbol{B}_{base}(x_i, y_i, z_i) \\ \boldsymbol{\tau} &= \frac{2\pi R l}{n \mu_0} \sum_{i=1}^{n} \boldsymbol{J}(\alpha, \beta, \gamma) \times \boldsymbol{B}_{base}(x_i, y_i, z_i) \end{aligned} \tag{9}$$

Here, $\{x_i, y_i, z_i\}$ are n evenly distributed points on the circumference of a cross-section of the center of the levitating magnet, perpendicular to its central axis. R and l are now the radius and height of the *levitating magnet*.

This approximation treats the permanent magnet as a thin polygon of electrical conductors instead of a current sheet, equivalent to applying the Laplace force law on

several linear wire segments. It achieves less than 0.07% relative error for $n = 100$ when compared to the solution of a continuous thin current loop (Wang and Ren, 2014). Although this approximation ignores the thickness of the levitating magnet, Section 3 shows that it is still adequate.

2.4 Translation & Rotation

Translation and rotation are modeled using Newton-Euler Equations of Motion. When the rotation is defined about the center of mass of the levitating magnet using Euler angles, (α, β, γ), and where linear and angular acceleration are given by $\boldsymbol{a} = [\ddot{x}, \ddot{y}, \ddot{z}]^T$ and $\boldsymbol{\alpha} = \dot{\boldsymbol{\omega}} = [\ddot{\alpha}, \ddot{\beta}, \ddot{\gamma}]^T$, respectively, the dynamics of the levitating magnet can be described as follows (Featherstone, 2014)

$$\begin{bmatrix} \boldsymbol{F} - \boldsymbol{F}_g \\ \boldsymbol{\tau} \end{bmatrix} = \begin{bmatrix} m\mathbf{I}_3 & \mathbf{0}_{3\times3} \\ \mathbf{0}_{3\times3} & \mathcal{I} \end{bmatrix} \begin{bmatrix} \boldsymbol{a} \\ \boldsymbol{\alpha} \end{bmatrix} + \begin{bmatrix} \mathbf{0}_{3\times3} \\ \boldsymbol{\omega} \times \mathcal{I}\boldsymbol{\omega} \end{bmatrix} \tag{10}$$

where

$$\mathcal{I} = diag\left(\left[\frac{1}{4}mR^2,\ \frac{1}{4}mR^2,\ \frac{1}{2}mR^2\right]\right)$$
$$\boldsymbol{F}_g = -mg\hat{\boldsymbol{e}}_z$$

Here, m is the mass of the levitating magnet, g denotes the gravitational constant, $\boldsymbol{F}$ and $\boldsymbol{\tau}$ are the magnetic force and torque acting on the magnet, respectively, and $\mathcal{I}$ is the inertia matrix (inertia of a disk). Note that the dependency of the force and torque on the position and rotation of the levitating magnet is assumed to be tacit.

2.5 Complete Model Description

The state and input vectors of the system are defined as

$$\boldsymbol{x} = [x, y, z, \alpha, \beta, \gamma, \dot{x}, \dot{y}, \dot{z}, \dot{\alpha}, \dot{\beta}, \dot{\gamma}]^T, \quad \boldsymbol{u} \in \mathbb{R}^{n_s \times 1}$$

where (x, y, z) and (α, β, γ) are the Cartesian coordinates and the Euler rotation angles of the center of gravity of the levitating magnet, and $\boldsymbol{u}$ is a vector containing all the solenoid currents, I_i.

Combining (1) / (2), (4), (5), (6), (8)/ (9), and (10), the entire system can then be compactly represented by

$$\dot{\boldsymbol{x}} = \mathbf{A}\boldsymbol{x} + \mathbf{B}f(\boldsymbol{x}, \boldsymbol{u}) \tag{11a}$$
$$\boldsymbol{y} = \mathbf{C}\boldsymbol{x} \tag{11b}$$

where

$$\mathbf{A} = \begin{bmatrix} \mathbf{0}_{6\times6} & \mathbf{I}_6 \\ \mathbf{0}_{6\times6} & \mathbf{0}_{6\times6} \end{bmatrix} \tag{11c}$$

$$\mathbf{B} = \begin{bmatrix} \mathbf{0}_{6\times6} \\ \mathbf{I}_6 \end{bmatrix} \tag{11d}$$

and

$$f(\boldsymbol{x}, \boldsymbol{u}) = \begin{bmatrix} m\mathbf{I}_3 & \mathbf{0}_{3\times3} \\ \mathbf{0}_{3\times3} & \mathcal{I} \end{bmatrix}^{-1} \left(\begin{bmatrix} \boldsymbol{F}(\boldsymbol{x}, \boldsymbol{u}) \\ \boldsymbol{\tau}(\boldsymbol{x}, \boldsymbol{u}) \end{bmatrix} - \begin{bmatrix} \boldsymbol{F}_g \\ \boldsymbol{w} \times \mathcal{I}\boldsymbol{w} \end{bmatrix} \right) \tag{11e}$$

where $\boldsymbol{\omega} = (\dot{\alpha}, \dot{\beta}, \dot{\gamma})$, I_n denotes identity matrices, $0_{n\times m}$ denotes zero matrices, and g is the gravitational constant. C is the measurement matrix, where choosing $C = I_{12}$ corresponds to full state measurements. Note again the slight abuse of notation to emphasize that the force $\boldsymbol{F}$ and torque $\boldsymbol{\tau}$ depend on the state (position and orientation) and the input (solenoid current) vector.

From (11), two models are defined :

Model 1: An accurate model, using (1) and (8) for the field and force calculations.

Model 2: A faster – but less accurate – model, using (2) and (9) for the field and force calculations.

3. SIMULATION STUDY

This section analyzes the effectiveness of the proposed models for use in control. The system under consideration is loosely based on typical tabletop levitation systems, with component specifications based on what is commercially available.

Three numerical simulation examples are presented:

Example 1: Testing *accuracy*, specifically on the force calculated on the levitating magnet for the different models.
Example 2: Testing *speed and accuracy* through LQR control of the proposed models compared to the filament model.
Example 3: Testing *advanced control*, using an MPC controller on Model 2 to achieve control objectives that are not possible with standard linear controllers.

3.1 Simulation Setup

The system is similar to the one shown in Fig. 1, consisting of four permanent magnets and four solenoids arranged to form the base, and a levitating magnet of a similar relative size. The component specifications are shown in Table 1. The set notation for the coordinates indicates the respective coordinate used to describe the center of the $i'th$ permanent magnet/solenoid.

Table 1. System parameters

Solenoids			
Symbol	Value	Symbol	Value
R [cm]	1	$\boldsymbol{x}$ [cm]	{3, 0, −3, 0}
l [cm]	0.8	$\boldsymbol{y}$ [cm]	{0, 3, 0, −3}
N	495	$\boldsymbol{z}$ [cm]	{0, 0, 0, 0}
Permanent Magnets			
R [cm]	1	$\boldsymbol{x}$ [cm]	{2, −2, −2, −2}
l [cm]	0.8	$\boldsymbol{y}$ [cm]	{2, 2, −2, −2}
J [T]	1.22	$\boldsymbol{z}$ [cm]	{0, 0, 0, 0}
Levitating Magnet			
R [cm]	2.5	m [g]	200 (with load)
l [cm]	0.5		
J [T]	1.22		

The system model was implemented in MATLAB using code from Moiseev (2008). Note the usage of equilibrium in the following: it is defined as the point $(x, y, z, \alpha, \beta, \gamma) = (0, 0, z_{eq}, 0, 0, 0)$ where the magnetic force cancels out the force of gravity. A simple line search finds that $z_{eq} = 5.06$ [cm] for this particular system configuration.

3.2 Example 1: Horizontal & Vertical Force

The accuracy of the force computations in each model was tested by calculating the forces produced by a single

permanent magnet/solenoid on a levitating magnet placed level to the base along a line described by $x \in [-7, 7]$, $y = 0$ and $z = z_{eq}$.

Fig. 3 shows the resulting vertical and horizontal forces, $\boldsymbol{F}_x$ and $\boldsymbol{F}_z$, produced by a permanent magnet, with excellent agreement between the two models. A finite element model (FEM) simulation was run using COMSOL Multiphysics to validate the model accuracy. The FEM solution, produced by a 2D axisymmetric model (hence only for $x = 0$), is also in agreement.

Fig. 4 displays the vertical and horizontal forces produced by a solenoid using Model 1, Model 2 and the filament model. The top graph reveal discrepancies between Model 1/2 and the filament model when using the actual solenoid's radius in the models. However, adjusting the radius according to (3) results in complete agreement between the models.

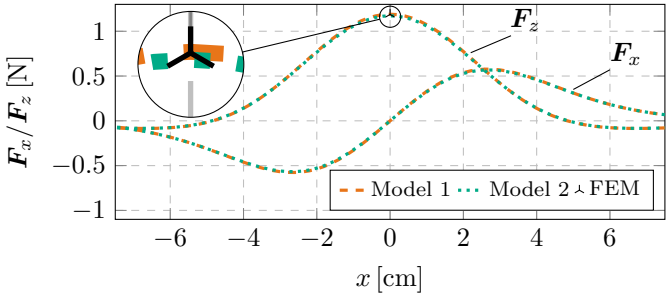

Fig. 3. Horizontal $\boldsymbol{F}_x$ and vertical force $\boldsymbol{F}_z$ acting on levitating magnet produced by a single magnet placed in $(0, 0, 0)$ when the magnet is placed level to the ground at $(x, 0, z_{eq})$ $\forall x \in [-7, 7]$ cm, $z_{eq} = 5.06$ cm.

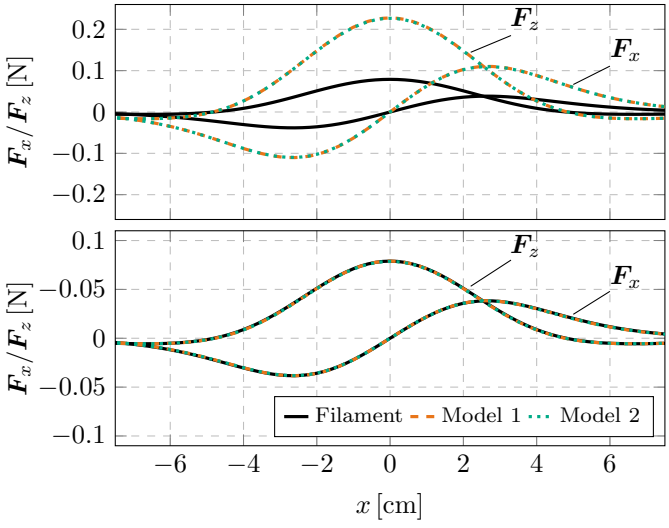

Fig. 4. Horizontal $\boldsymbol{F}_x$ and vertical force $\boldsymbol{F}_z$ acting on levitating magnet produced by a single solenoid placed in $(0, 0, 0)$ when magnet is placed level to the ground at $(x, 0, z_{eq})$ $\forall x \in [-7, 7]$ cm, $z_{eq} = 5.06$ cm.
Top: Using radius R in the models. **Bottom**: Using adjusted radius $\widehat{R}$ (3) s.t. $\widehat{R}/R = 0.5789$.

3.3 Example 2: LQR Stabilization

To assess the computational speed of the proposed models, a comparison with the filament model was conducted when controlling the systems using a standard linear-quadratic regulator (LQR). The LQR controller was designed with linear system matrices obtained from linearizing the models around the equilibrium point $(0, 0, z_{eq})$. The LQR gains were determined by tuning the LQR cost matrices until satisfactory performance was achieved. Note that the goal is not to optimize control performance, but to highlight both the feasibility of designing a controller, as well as the accuracy and computational speed of the proposed models, so control parameters are omitted for brevity.

The systems were stabilized from the inital point $x(t = 0) = [-0.01, 0.01, 0.08, \pi/10, -\pi/10, 0 \ldots, 0]^T$ towards equilibrium using the LQR controllers with full state feedback. The results using Runge-Kutta-4(5) are shown in Fig. 5. The proposed models' trajectories closely match the filament model. Table 2 shows the simulation time and the total RMSE when comparing the two models to the filament model. The RMSE is relatively small for both models considering the relative magnitude of the states. However, the simulation time is orders of magnitude smaller for Model 2 than Model 1 and the filament model, offering real-time simulation, since it is solved in $< 1\,s$ on a low-end laptop.

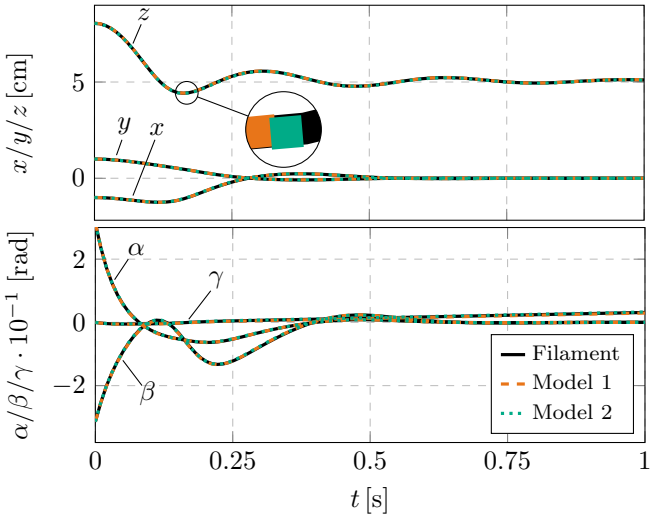

Fig. 5. Results from using an LQR controller on the filament model and Model 1 & 2.

Table 2. Simulation time & relative error

Model	Simulation Time (relative)	RMSE (total)
Fillament Model	1.0000	N/A
Model 1	0.5690	0.0042
Model 2	0.0113	0.0048

3.4 Example 3: MPC Stabilization and Rotation Control

One key limitation of this type of magnetic levitation system is the difficulty of rotating the levitating magnet around its own axis due to uniform axial polarization and geometrical symmetry. This is apparent when considering the linearized model, where γ and $\dot{\gamma}$ are uncontrollable states, making it impossible to design a suitable linear controller based on the linearization alone.

This problem can be solved by using a more advanced controller, such as a nonlinear model predictive controller (NMPC). In general, NMPC allow for constrained MIMO control that, for many applications, yield more novel control than with standard linear controllers. Although

γ cannot be controlled when the levitating magnet is in equilibrium, it can be controlled indirectly by first rotating the magnet around one of the other two axis. This is shown in Fig. 6, where a CasADi implementation of an NMPC using Model 2, Runge-Kutta 4 and multiple-shooting, is used to control Model 2. The levitating magnet is initialized with $\gamma(t=0) = 0.25\,[\text{rad}]$, with the remaining states in equilibrium.

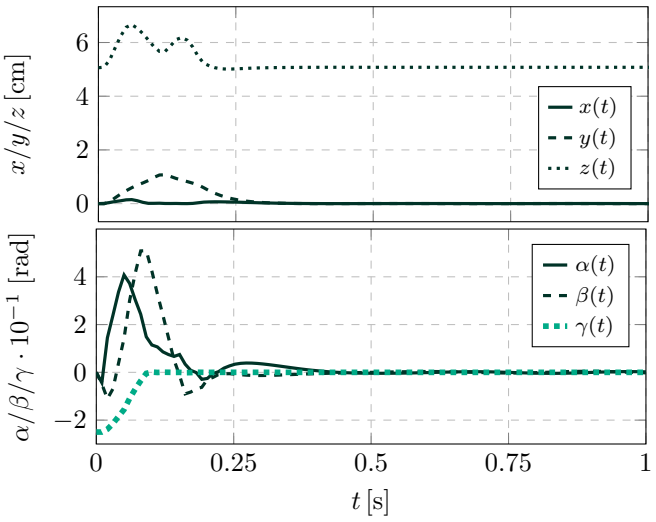

Fig. 6. Results using NMPC with model 2.

The figure shows how the NMPC controller stabilizes γ by controlling the other states in a "wobble"-like maneuver. This is novel behavior that is made possible due to the NMPC enabled by the relatively lightweight and accurate models presented in this manuscript.

4. CONCLUDING REMARKS

We have presented two models for advanced control applications in a specific class of magnetic levitation systems. The system can be considered a type of planar magnetic motor that maintains a single permanent magnet floating above a base composed of permanent magnets and electromagnetic solenoids. Model 1, adapted directly from existing literature on semi-analytical solutions for the magnetic fields of ideal solenoids, provides a highly accurate model when compared to a standard filament model. Meanwhile, Model 2 employs a simple discretization for near real-time model performance. Simulation studies reveal that both models exhibit comparable accuracy to a filament model implementation, but with up to a 98% reduction in computational time for Model 2, demonstrated using a linear-quadratic regulator (LQR) for stabilization. We also showcased novel control behavior enabled by the use of Model 2 in a nonlinear model predictive controller (NMPC).

Further work should focus on using the proposed models to demonstrate real-time optimal control of a physical implementation of the magnetic levitation system. This necessitates the design of observers based on these models to estimate system states when not directly measurable (e.g., when magnetic measurements are used), and the implementation of a suitable parameter identification process for fine-tuning the models.

Acknowledgments — The authors would like to thank D. Varagnolo and the reviewers for valuable discussions and suggestions.

REFERENCES

Berkelman, P. and Dzadovsky, M. (2013). Magnetic levitation over large translation and rotation ranges in all directions. *IEEE-ASME Transactions on Mechatronics*.

Bächle, T., Hentzelt, S., and Graichen, K. (2013). Nonlinear model predictive control of a magnetic levitation system. *Control Engineering Practice*, 21(9), 1250–1258.

Carneiro, P., Soares dos Santos, M.P., Rodrigues, A., Ferreira, J.A., Simões, J.A., Marques, A.T., and Kholkin, A.L. (2020). Electromagnetic energy harvesting using magnetic levitation architectures: A review. *Applied Energy*, 260, 114191.

Cho, D., Kato, Y., and Spilman, D. (1993). Sliding mode and classical controllers in magnetic levitation systems. *IEEE Control Systems Magazine*, 13(1), 42–48.

Derby, N. and Olbert, S. (2010). Cylindrical magnets and ideal solenoids. *American Journal of Physics*.

Featherstone, R. (2014). *Rigid body dynamics algorithms*. Springer.

González, M.A. and Cárdenas, D.E. (2020). Analytical expressions for the magnetic field generated by a circular arc filament carrying a direct current. *IEEE Access*, 9, 7483–7495.

Husa, P.L., Saunders, B.D., Suesser, B.E., and Petruska, A.J. (2020). Optimal current shell approximation for solenoids of rectangular cross-section. *AIP Advances*.

Jansen, J., Smeets, J., Overboom, T., Rovers, J., and Lomonova, E. (2014). Overview of analytical models for the design of linear and planar motors. *IEEE Transactions on Magnetics*, 50(11), 1–7.

Lemarquand, G., Lemarquand, V., Babic, S., and Akyel, C. (2009). Magnetic field created by thin wall solenoids and axially magnetized cylindrical permanent magnets.

Moiseev, I. (2008). Elliptic functions for matlab and octave. `https://github.com/moiseevigor/elliptic`.

Rahmani Dabbagh, S., Alseed, M.M., Saadat, M., Sitti, M., and Tasoglu, S. (2021). Biomedical applications of magnetic levitation. *Advanced NanoBiomed Research*, 2, 2100103.

Ravaud, R., Lemarquand, G., Babic, S., Lemarquand, V., and Akyel, C. (2010). Cylindrical magnets and coils: Fields, forces, and inductances. *IEEE Transactions on Magnetics*.

Sadiku, M.N. and Nelatury, S. (2001). *Elements of electromagnetics*, volume 428. Oxford university press New York.

Trumper, D.L., Olson, S.M., and Subrahmanyan, P.K. (1997). Linearizing control of magnetic suspension systems. *IEEE Transactions on control systems technology*, 5(4), 427–438.

Uno, M. (2016). Chuo shinkansen project using superconducting maglev system. *Japan Railway & Transport Review*, 68, 14–25.

Wang, Z.J. and Ren, Y. (2014). Magnetic force and torque calculation between circular coils with nonparallel axes. *IEEE Transactions on Applied Superconductivity*, 24, 1–5.

Zhang, Y., Leng, Y., Liu, J., and Tan, D. (2019). Comparison of magnetic force calculation on permanent magnets with models of equivalent magnetic charge and magnetizing current. *Journal of Magnetics*.